Progress Report - July 31, 1996
NASA Grant # NCC-1-214

Interpretation of Lidar and Satellite Data Sets using a Global Photochemical Model

Principal Investigator and grantee:	Dr. Thomas Zenker
Co-Investigator:	Dr. Thomas Chyba
Institution:	Hampton University Hampton, VA 23668

Report period:	08/95-07/96

1. Accomplishments

The status in the beginning of the report period was that the existing General Circulation Model (GCM) was running with a chemistry module compiled for stratospheric simulation studies. The chemistry simulation was not working sufficiently in the troposphere and any tropospheric trace gas sources or dry deposition sinks were not yet incorporated.

The current status concerning the chemistry module is that

- the chemistry simulation has been modified to also simulate the chemistry in the troposphere with resulting mixing ratios close to other model simulations as described in Olson et al. (1996).
- The mechanism to incorporate trace gas source, e.g. testing for NO_x, and dry deposition sinks, testing for H_2O_2, CH_3OOH, O_3, HCHO, HNO_3, and NO_2, are incorporated and is currently being tested.

Existing model and development versions:

- The full GCM model, currently still running with the original stratospheric chemistry module.
- An off-line version of the GCM, i.e. wind and photolysis rates are pre-calculated and prescribed in read-in arrays. Here, the current modification are incorporated and are under test.
- A box model version of the modified chemistry module for developments and first tests of new modifications.
- A box model with same chemistry simulated but flexible partitioning and integration methods for test purposes of those.

Several NASA scientist working in a joint effort on the development of the GCM at the NASA Langley Research Center which is funded through different grants. In particular three scientists, including the grantee, are working on the tropospheric chemistry part. Consequently the entire tropospheric development was not accomplished by the grantee alone. The grantee's work focused mainly on three areas:

- Trace gas sources and dry deposition
- Method to introduce a NO source instead of a NO_x source
- Investigating integration methods

These three areas and accomplishments are discussed in more detail:

- Tropospheric chemistry, dry deposition and trace gas sources

A mechanism for computing trace gas production and loss terms caused by trace gas source and dry deposition fields has been incorporated in the off-line GCM version and is in a test phase.

Mechanism: The calculation of deposition and source terms is using prescribed deposition velocity (currently for O_3, HCHO, H_2O_2, CH3OOH, NO2, and HNO_3) and source flux arrays (currently for NO_x). Deposition velocities (or the associated transport resistance, see below) and source fluxes are the form in which , in general, the data are available in literature.

The deposition velocity (v_{dep}) is defined as (Warneck 1990)

$$v_{dep} = 1 / (R_g + R_s)$$

where R_g and R_s are the ground and surface resistance, respectively, using the assumption that the surface flux is equal to the ground flux. R_g reflects the transport resistance in the lowest few centimeters adjacent to a surface, and R_s is surface specific, e.g. surface could be bare ground or leaves. Deposition velocities are species and surface specific. In this test phase values from Müller (1992) for O_3, HCHO, H_2O_2, CH3OOH, and HNO_3 are used. The velocities for the different species are assigned to different vegetation classes. An longitude-latitude array has been generated using the NCAR vegetation database ds.769 overlaid with snow and ice data used in the GCM. The resulting data array groups the earth surface into seven classes: ice/snow, water, bare ground, grass/shrubs, grass/shrubs/trees, non-tropical forest, and tropical forest (Figure 3) on a 0.5x0.5 degree resolution. The deposition velocities are assigned to this database and then averaged to the 128x64 model grid array. Resulting deposition arrays for HNO_3, H_2O_2, and O_3 are shown in Figure 4a-c.

An additional transport resistance has to be introduced for the model surface interface, i.e. the column between surface and lowest model layer, in order to scale the deposition velocity which is defined at ground level (v_{dep}) to a deposition velocity (v_{dep}*) at the lowest model layer. This surface interface resistance R_d is the inverse of the model air/surface interaction coefficient D_r (Model description; Stull 1988):

$$R_d = 1 / D_r = 1 / (C_d * M)$$

where C_d and M are the drag coefficient and a mean wind velocity, respectively. V_{dep}* is then (e.g. Levy et al. 1985)

$$v_{dep}^* = 1 / (R_s + R_g + R_d) = v_{dep} \times (1 - v_{dep} / D_r)$$

D_r, i.e. C_d and M, arrays will be provided from the transport routine of the model in order to calculated the modified deposition velocity v_{dep}* and associated loss rate in the chemistry routine. M is differently calculated for stable and unstable planetary boundary layers. Currently, for D_r is assumed some global averaged number for the off-line test version of the model.

The conversion of deposition velocities and sources fluxes into loss and production terms is performed as

$$L_{dep}[1/\text{sec}] = v_{dep} * /(dz/2)$$

$$P_{src}[\text{molec}/\text{cm}^3/\text{sec}] = F_{surface}/(dz/2)$$

$$P_{src}[\text{molec}/\text{cm}^3/\text{sec}] = F_{cell}/dz$$

where dz is the thickness of the model layer. For fluxes ad losses from/to the ground surface one has to use the column height between ground and the actual height of the layer center, that is dz/2, where the model calculations are performed. For sources generated inside a certain cell volume not originating from the surface, like the NO source from lightning or aircraft emissions, the thickness of the entire layer dz has to be used. As example, the difference between one-day model runs with and without deposition is shown for the resulting H_2O_2 and O_3 mixing ratios in the lowest model layer in Figure 5. As expected from the deposition velocity arrays (compare Figure 4), the major losses appear over land and water and over land for H_2O_2 and O_3, respectively.

Status: The NO_x source and deposition terms added to the off-line GCM version are still under test.

- A method to introduce NO sources instead of NO_x sources to the chemical routine.

Problem: Since combustion processes emit mostly NO it would be more appropriate to introduce an NOx source in form of NO into a chemical model simulation. During daytime, NO is oxidized to NO2 and NO3 and rapidly recycled to NO through photolytic decomposition of NO_2 and NO_3 forming a catalytic chain reaction. Especially in the limit of nighttime conditions, i.e. under missing photolytic decomposition of NO_3 to NO2 and NO_2 to NO, introducing NO_x in form of NO_2 instead of NO would miss the oxidation step NO + O_3 and its associated loss rates for ozone. In the limit of daytime conditions it makes primarily no difference of adding either NO_2 or NO because the catalytic NO-NO_2 cycle has a very high gain (chain length) in the order of several hundred recycles before NO/NO_2 is lost into long lived reservoirs like HNO_3, HNO_4, or PAN, and the difference of transitions NO→NO_2 and NO_2→NO can only be maximal one of total hundreds per added NO or NO_2. The transition between day and nighttime conditions is more complicated while the chain length of the NO/NO catalytic cycle drops to zero and the oxidation to NO_3 and the loss to N_2O_5 increases. Nevertheless, since all this transitions are faster than tens of seconds and fast compared to integration time steps of typically dt≥900s for global or regional model simulations, the NO-NO_2-NO_3 systems will be in photochemical equilibrium (PCE) and can be analyzed under fixed conditions, i.e. fixed mixing ratios resulting from the partitioning of NO_x, for a particular time t. A NO source cannot simply be added as NO to the chemical system because NO-NO_2 or NO_2-NO_3 already appear in PCE after partitioning and the fast relaxation processes, esp. in catalytic chains, cannot be resolved under a time step of dt.

Method: The chemical system is analyzed for a certain time t, this is no time step $t_0 \rightarrow t_1$ is performed but the flow of chemical reaction paths is analyzed based on the branching ratios between competing reactions under fixed species concentrations. The total sum of a species loss or production from reactions inside a feedback loops, like $NO \Leftrightarrow NO_2$, can be parameterized in its loss or originating reaction times the gain (chain length) of the feedback loops. E.g. the loss of O_3 from its reaction with NO ($LO_3(NO+O_3)$) per initial NO molecule (O_3 yield per NO) can be written as the branching ratio of NO reacting with O_3 against the sum of all possible NO reactions (α_{NO+O3}) times the $NO \Leftrightarrow NO_2$ loop gain G_{12} (indices 1 and 2 symbolize NO and NO_2; G_{23} will be the loop gain of $NO_2 \Leftrightarrow NO_3$), see Equ. 2. The lower of the indices of LO_3 symbolizes its yield per initial molecule X, e.g. NO, and the upper one symbolizes the chemical system analyzed, e.g. here the $NO \Leftrightarrow NO_2$

$$LO_3\left(NO+O_3\right)\Big|_{NO}^{NO\leftrightarrow NO_2} = G_{12} \times \alpha_{NO+O_3}$$

Equ. 2 O_3 loss per initial NO from $NO+O_3$ inside the $NO \Leftrightarrow NO_2$ catalytic chain loop.

$$LO_3\left(NO+O_3\right)\Big|_{NO_2}^{NO\leftrightarrow NO_2} = G_{12} \times \alpha_{jNO_2} \times \alpha_{NO+O_3}$$

Equ. 1 O_3 loss per initial NO_2 from $NO+O_3$ inside the $NO \Leftrightarrow NO_2$ catalytic chain loop.

loop (no feedback from NO_3 included). Equ. 1 shows the O_3 loss of this reaction yielded per initial NO_2. During daytime, (and for not too high O_3 concentrations) α_{NO+O3} and α_{jNO2} are close to one (>0.99), thus LO_3 either per initial NO or NO_2 result in the same value, this is it makes primarily no difference adding NO or NO_2 during daytime. It turns out that the entire O_3 loss yield per initial molecule X (X=NO,NO_2 ,...) can be parameterized into the form of Equ. 3. F,g, and h are product terms of branching ratios α describing the path from the initial molecule to the target reaction (e.g. $NO+O_3$ or NO_2+O_3, see examples in Equ. 2and Equ. 1), and G_{123} is an additional overall loop gain arising from the coupling of the two feedback loops $NO \Leftrightarrow NO_2$ and $NO_2 \Leftrightarrow NO_3$.

$$LO_3\Big|_X^{NO\leftrightarrow NO_2\leftrightarrow NO_3} = G_{123} \times \left\{ G_{12} \times f_X\left(\alpha_i\right) + G_{23} \times g_X\left(\alpha_j\right) + G_{12} \times G_{23} \times h_X\left(\alpha_k\right) \right\}$$

Equ. 3 Total O_3 loss per initial X (X=NO,NO_2,..) from the $NO \Leftrightarrow NO_2 \Leftrightarrow NO_3$ coupled catalytic loops.

Model incorporation: The chemical routine (chemical solver) is initialized with mixing ratios of transported long lived families, i.e. groups of species, and the source flux arrays. The initial mixing ratio of a species family is then the result of chemical integration from the prior time step, plus the modification from transport calculations, plus an additional amount calculated from the source flux. The chemical solver can be seen separated in the partitioning of the long lived families into their shorter lived members, the estimation of chemical tendencies based on the chemical interaction of the partitioned species, i.e. computing of production and loss terms, and the final integration of the families (Figure 1). The partitioning step is in general iterated to gain stable solutions for, e.g. radicals like OH or NO while their production and loss terms depend strongly on each other.

The new approach introduces an additional subroutine which analyses product yields of processes fast compared to time step dt, particular in this case, the O_3 yield of the NO-NO_2-NO_3 catalytic cycle per NO or NO_2 added. This analysis would be placed after the partitioning (see Figure 1, shaded box). Here, the ratio RLO_3 of the O_3 loss yield per NO over the loss yield per NO_x in PCE (i.e. $NO/NO_x=a$, $NO=aNO_x$, $NO_2=(1-a)NO_x$) will be calculated (see Equ. 4b); NO_x in PCE, this is the NO/NO_2 PCE ratio for daytime, and NO_2 for nighttime. RLO_3 can be used to correct the loss term LO_3 of the chemical tendency for O_3 (see Equ. 4c) which will be, as usual, in a first step estimated for dt based on total NO_x in PCE (see Equ. 4a). I.e. the fraction of LO_3 originating from the NO source will be multiplied by RLO_3, gaining a final corrected chemical tendency for O_3.

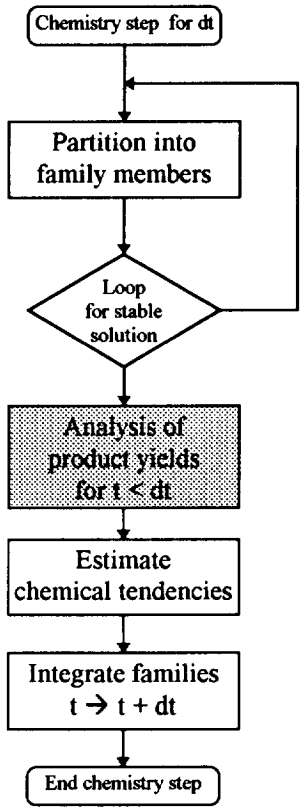

Figure 1.

Chemical solver

$$NO_x^{tot} = NO_x^{init} + NO_x^{source}$$

$$RLO_3 = LO_3\big|_{NO}^{NO \leftrightarrow NO_2 \leftrightarrow NO_3} \Big/ LO_3\big|_{NO_x inPCE}^{NO \leftrightarrow NO_2 \leftrightarrow NO_3}$$

$$LO_3\left(NO_x^{tot}, dt\right) = LO_3\left(NO_x^{tot}, dt\right) \times \left\{ \frac{NO_x^{init}}{NO_x^{tot}} + \frac{NO_x^{source}}{NO_x^{tot}} \times RLO_3 \right\}$$

Equ. 4

a) total NO_x = initial NO_x (from prior time step) + NO_x source.

b) Ratio of O_3 loss yield per NO over yield per NO_x (in PCE) for the $NO \Leftrightarrow NO_2 \Leftrightarrow NO_3$ catalytic chain loops.

c) Correction of the loss term of the O_3 tendency which has been calculated for dt and NO_x^{tot} which will correct the O_3 loss yield for introducing a NO_x source in form of NO.

Status: To test Equ. 4.b, RLO_3 has been calculated for mixing ratios of species compiled in box model runs initialized with 4 standard sets of species mixing ratios, altitude, and temperature: the 4 "IPCC cases" marine", "land", "plume-X", and "free-troposphere" which were used for model inter-comparisons (Olson et al. 1996). Results are shown in Figure 6. As expected, RLO_3 is equal to one for daytime. RLO_3 significantly becomes >1 when the NO_3 photolysis rate drops below 10% of its noon value. At nighttime there is no photolytic decomposition of NO_2 and NO_3 recycling NO ($\rightarrow$ $G_{12}=G_{23}=G_{123}=1$). Thus the maximum O_3 loss per initial NO and NO_2 is 2 and 1 (nominator and denominator of Equ. 4.b), respectively, through reactions $NO+O_3$ and NO_2+O_3. Since NO_2+O_3 is competing against $NO_2+NO_3 \rightarrow N_2O_5$ the nominator and denominator of Equ. 4b will range between 1-2 and 0-1, resp. (neglecting $NO+NO_3$), and RLO_3 will become >2. The difference in amplitude of RLO_3 between cases "land" and "marine" are due to different species mixing ratios, while the higher amplitude for "plume-X" and "free-troposphere" is due to lower temperatures and associated more favorable losses into the N_2O_5 reservoir. Increasing RLO_3 values during night are associated with increasing NO_3 mixing ratios (not shown) causing increasing losses towards N_2O_5.

In a next step this needs to be added and tested in the off-line version of the GCM. Likely, this analytical method can also be used to calculate, e.g. OH, HO_2, or O_3 yields from fast non-methan hydrocarbons (NMHC) reaction chains when adding NMHC chemistry to the model.

- Comparison of integration steps

Integration in the chemical solver using 900 second time steps show variations after a compared to 10 second fine step integration, e.g. after 5 days the differences for diurnal means can be in the order of 10% depending on initial conditions (IPCC cases). In the model version used for development, generally, for integration time step $dt>5\tau$ (τ is lifetime of species X), $0.2\tau<dt<5\tau$, and $dt<0.2\tau$ the integration over dt is calculated using photochemical equilibrium (PCE) assumption, implicit, and forward Euler integration

$$X(t_1) = \left(P - L \times X(t_0)\right) \times dt$$

$$X(t_1) = \frac{P \times dt + X(t_0)}{1 + L \times dt}$$

$$X(t_1) = X(t_0) + \left(P/L - X(t_0)\right) \times \exp(-L \times dt)$$

Equ. 5 Integration steps: "forward Euler", "implicit", and "exponential", respectively

steps, respectively (see Equ. 5). All are functions of the production (P) and loss (L) terms. For a chemical solver as shown in Figure 1 with an iteration loop for the partitioning section the resulting terms P and L are generated for the time t_0. The "correct" values for P and L would be some integral of P(t) and L(t) between t_0 and t_1 which is unknown since calculations are only performed for times in step of dt. It has been investigated how integration results vary if one uses $P(t_1)$ and $L(t_1)$ instead of $P(t_0)$ and $L(t_0)$ or some average of them. P and L for t_1 can be calculated if one adds an additional iteration loop including the estimate of tendencies and the integration of families (compare Figure 1). The integration results for dt are compared to a fine step integration using forward Euler integration in steps of $\tau/100$ which don't differ anymore from results using even finer time steps and are assumed to be "correct" solution with error <<1%. Different P/L shapes were assumed between t_0 and t_1 as illustrated in Figure 2. The envelopes of the resulting ratios between dt step integration and $\tau/100$ step integration are shown in Figure 7-9 as function of τ. Positive numbers in these graphs mean, the dt integration overestimates values for $X(t_1)$, while negative numbers indicate an underestimation. It turns out that forward Euler and implicit integration steps for the above defined time domains using P and L of t_0 general underestimate any results while using P and L of t_1 overestimate any results for $X(t_1)$ (compare Figure 7, Figure 8). This general trent could also be verified in box model runs using these two possible sets of P and L values. Using an exponential integration step (this is the correct solution for a P/L shape stepping at t_0 to its final values $P/L(t_1)$ and staying constant over dt and only for this shape!) gives similar results as the implicit step with slightly smaller error for the implicit one (the results using the exponential step are not displayed). (Note, that the large errors for the PCE values originate from concave shape calculations. A PCE state can hardly be reach if the change

of the P/L value increases in time. At some point he system cannot anymore follow the changing P/L value fast enough.)

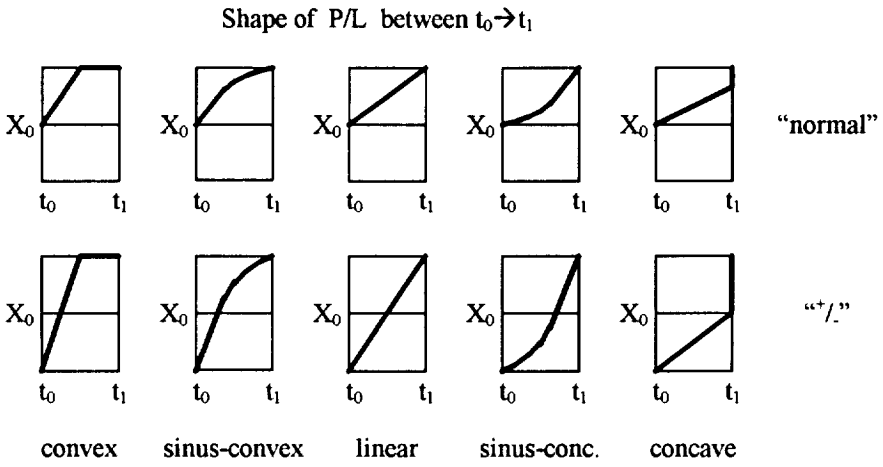

Figure 2 Shapes of (production)/(loss)=P/L term steady state values assumed between integration time step t_0 and t_1. In "normal" the species mixing ratio at t_0 is at its equilibrium value $P/L(t_0)$, in "+/-" cases the P/L value crosses the start value X_0. Shapes with opposite signs (mirrored at $y=X_0$ will just flip sign of integration results. Concave and sinus-concave cases reflect the situation after sunrise and after noon where P/L values generally change increasingly. Convex and sinus-convex cases reflect cases befor noon and before sunset where changes in P/L decrease. Approximately linear changes

Figure 9 show the envelope of results choosing $P=P(t_1)$ and $L=L(t_1)$ for the linear and convex P/L shapes, and $P=(P(t_0)+P(t_1))/2$ and $L=(L(t_0)+L(t_1))/2$ for the concave shapes, additionally implicit steps are used for $dt>5\tau$ instead of PCE calculation in case of concave shapes. The error band indicated by the envelope curves is much smaller than for the calculation using either P and L only as function of t_0 or t_1. A more sophisticated exponential integration step, consisting of three different exponential terms which are function of $P(t_0)$, $P(t_1)$,$L(t_0)$, and $L(t_1)$ has been found which can compute results with much lesser errors than any other integration step discussed here. But two parameter have to be optimized for the specific shape of P/L.

The point is, one can possibly improve the performance of the integration step by using not only production and loss term (P and L) as function of t_0 but also of t_1, as discussed above. But one has to introduce the mentioned outer iteration loop in the chemical solver routine which would mean that more computing time is used. Additionally, one has to setup criteria that define for what time period (associated with different P/L shapes in time) which kind of averaged value of P and L need to be used (two different types might be sufficient). This might be possible but has not yet been tested thoroughly with the box model, and improvements could not be verified yet.

2. Comparison to proposed work

The work proposed for the report period was mainly focused on preparing data arrays from field experiment, e.g. O_3 LIDAR data, and starting a data-model comparison. The status of the tropospheric part of the model in the beginning of this report period was far from starting reasonable comparisons, e.g. the at this time incorporated basic chemistry was optimized for the stratosphere requirements and needed to be modified to work in the troposphere, neither were surface source and sink (dry deposition) terms incorporated which are essential for global tropospheric simulations. It seemed therefor to be more important first to focus on the model development to reach a status of the model where reasonable data-model comparison could be started.

3. Milestones for the last grant year 08/96-07/97

- Model development
  - * Finalize testing of deposition and NO_x source terms
  - * Incorporate NO source instead of NO_x source
  - * Incorporate CO source and dry deposition, and also for hydrocarbons in time when associated chemistry will be incorporated.
  - * Start to incorporate NMHC chemistry.
  - * Look more into whether integration methods for chemical tendencies could be improved.
  - * Develop and test above tools in off-line version and incorporate them in the full GCM version.
- Data-model comparison
  - * Prepare software tools and data arrays to use TOMS residual ozone database and the LaRC ozone sonde database for climatological model evaluations. Start model evaluations
  - * Build up database of regional/large scale experiments, e.g. TRACE-A/SAFARI-92 or PEM-West, for model comparison.
  - * Use prescribed ECMWF or ECM wind fields with off-line GCM version for comparison with regional field data sets in specific time periods.

Figure captions

Figure 3. Vegetation classes grouped using the NCAR Olson ds.769 vegetation database, 0.5x0.5 degrees (http://www.ucar.edu/dss/datasets/ds769.0.html) and snow/ice data used in the GCM.

Figure 4. Deposition velocity grid arrays for **a)** HNO_3, **b)** H_2O_2, and **c)** O_3.

Figure 5. Difference of **a)** H_2O_2 AND **b)** O_3 mixing ratios in the lowest layer between 1-day 3D model runs with and without deposition terms.

Figure 6. Correction factor RLO_3 for correcting the O_3 loss term for adding a NO_x source in form of NO instead of NO_x. RLO_3 is calculated following **Equ. 4b** for the four "IPCC cases". Additionally, the NO_2 and NO_3 photolysis rates are displayed.

Figure 7. Ratio of integration results as function of lifetime τ of a species X. Used were P=P(t0) and L=(t_0). Integration performed in one time step dt=τ over results in hundert time steps of τ/100. Prescribed shape of P/L in time according to **Figure 2** are used. The envelope of the results for every shape is shown, (∇) for all shapes, (X) for shapes excluding "+/-" cases and the concave cases.

Figure 8. Same as **Figure 7** but using P=P(t_1) and L=L(t_1).

Figure 9. Same as **Figure 7** but using P=(P(t_0)+P(t_1))/2 and P=P(t_1) for concave cases and for all others, respectively. (Same for L). For concave cases no PCE calculation is used but implicit steps for the entire range of dt>τ/5.

References

Levy II, H., J. D. Mahlman, and W. J. Moxim, Tropospheric Ozone: The role of transport, *J. Geophys. Res.*, **90**, D2, 3753-3772, 1985.

Müller, J.-F., Geographical distribution and seasonal variation of surface emissions and deposition velocities of atmospheric trace gases, *J. Geophys. Res.*, **97**, D4, 3787-3804, 1992.

Olson, J. R., et al., Results from the IPCC photochemical model intercomparison (PhotoComp): Some insights into tropospheric chemistry, *J. Geophys. Res.*, submitted 1996.

Stull, R. B., An introduction to boundary layer meteorology, *Kluwer Academic Publishers, Dordrecht*, ISBN 90-277-2769-4, 1988

Warneck, P., Chemistry of the Natural Atmosphere, Academic Press Inc, San Diego CA, ISBN 0-12-735630-4, 1988.

Vegetation Classes, 0.5x0.5 degrees (based on Olson NCAR-ds.769)

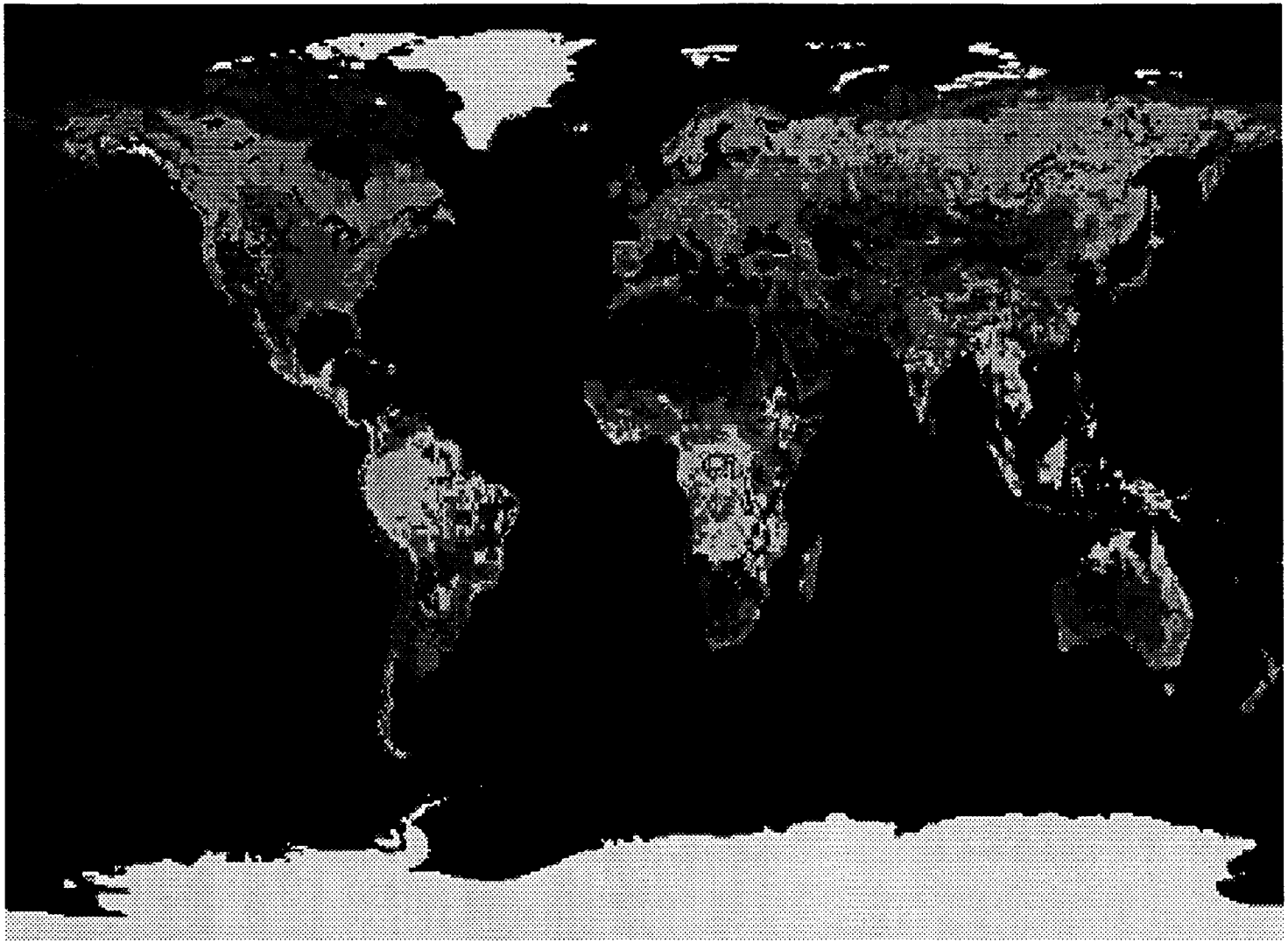

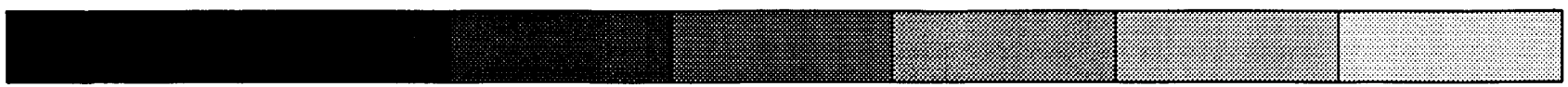

fig 3

HNO3 (JUL)-dep.-velocity, 2.8x2.8 deg (based on ds.769 & LARC snow/ice)

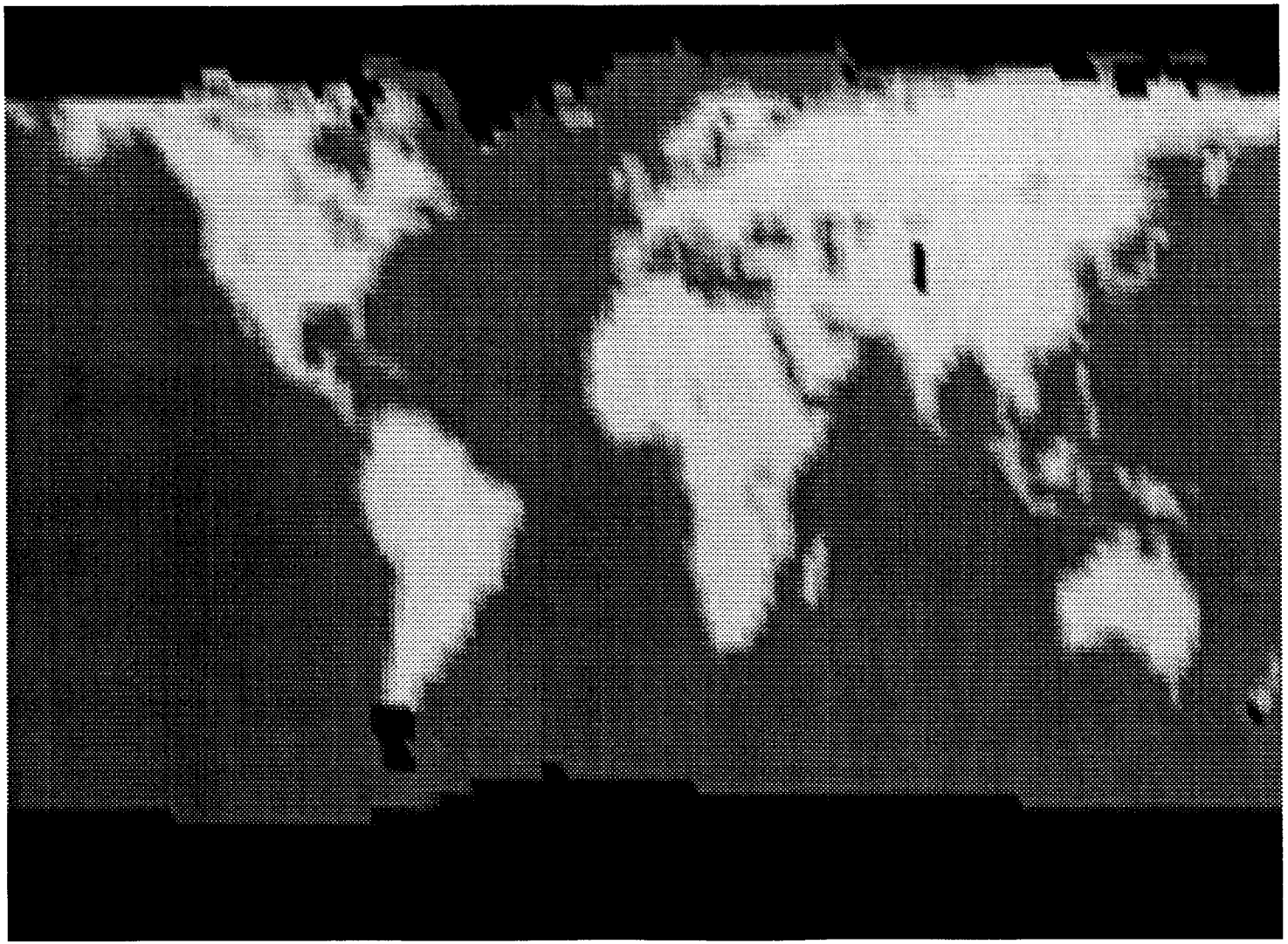

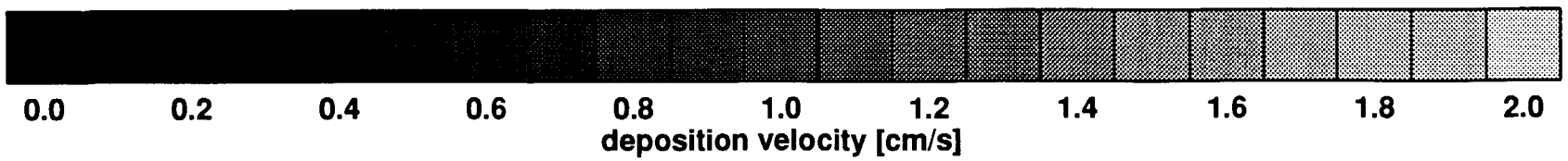

Fig 4a

H2O2 (JUL)-dep.-velocity, 2.8x2.8 deg (based on ds.769 & LARC snow/ice)

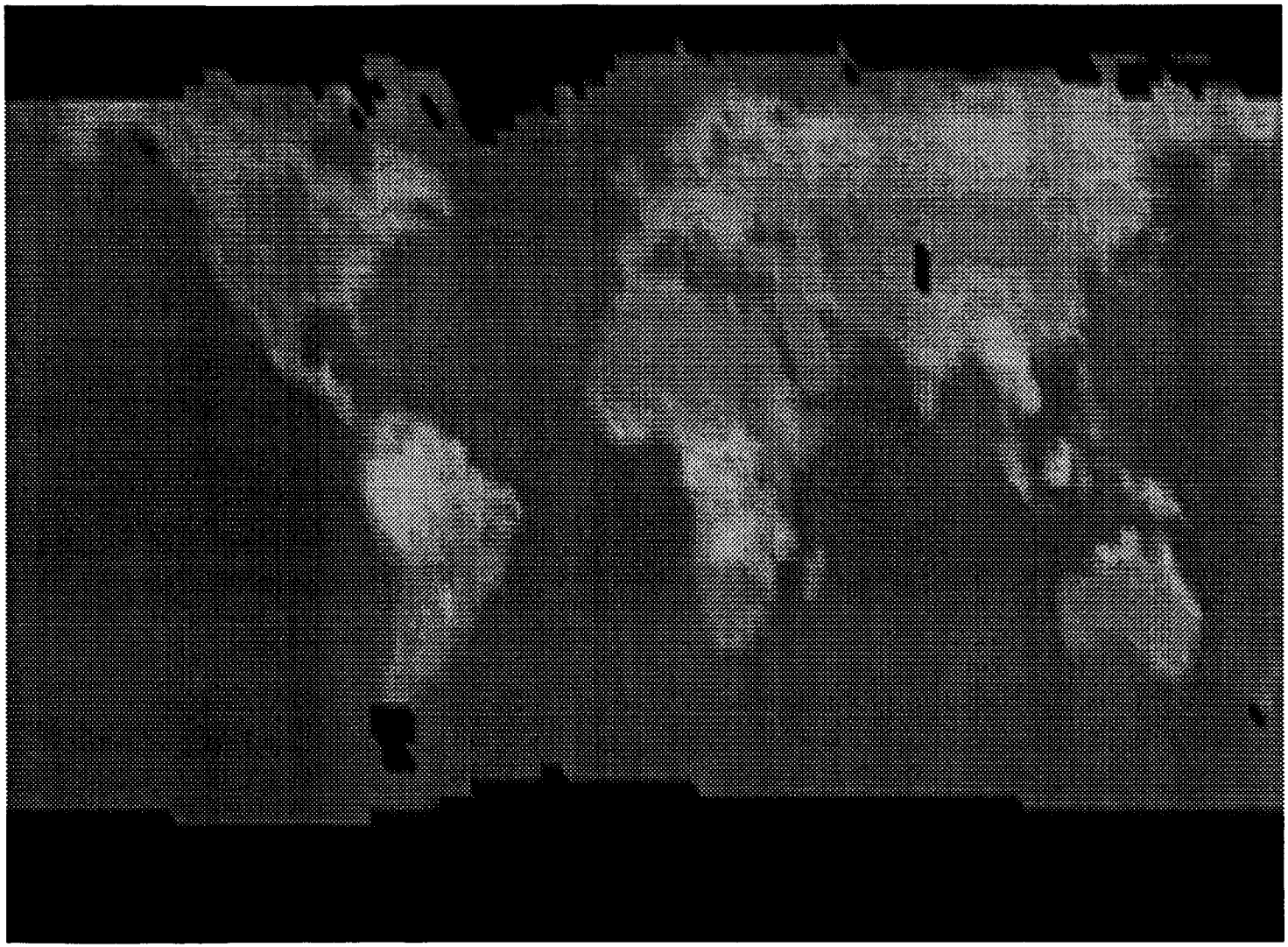

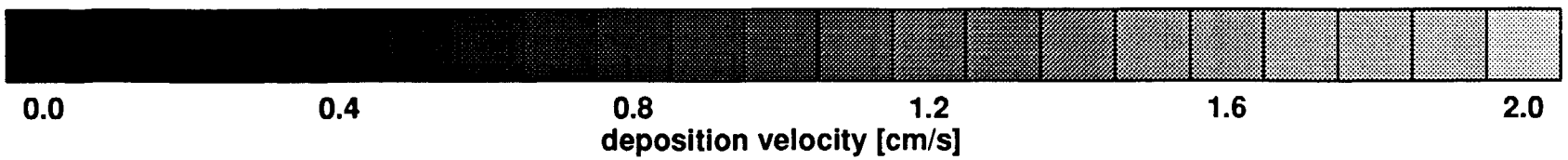

94 845

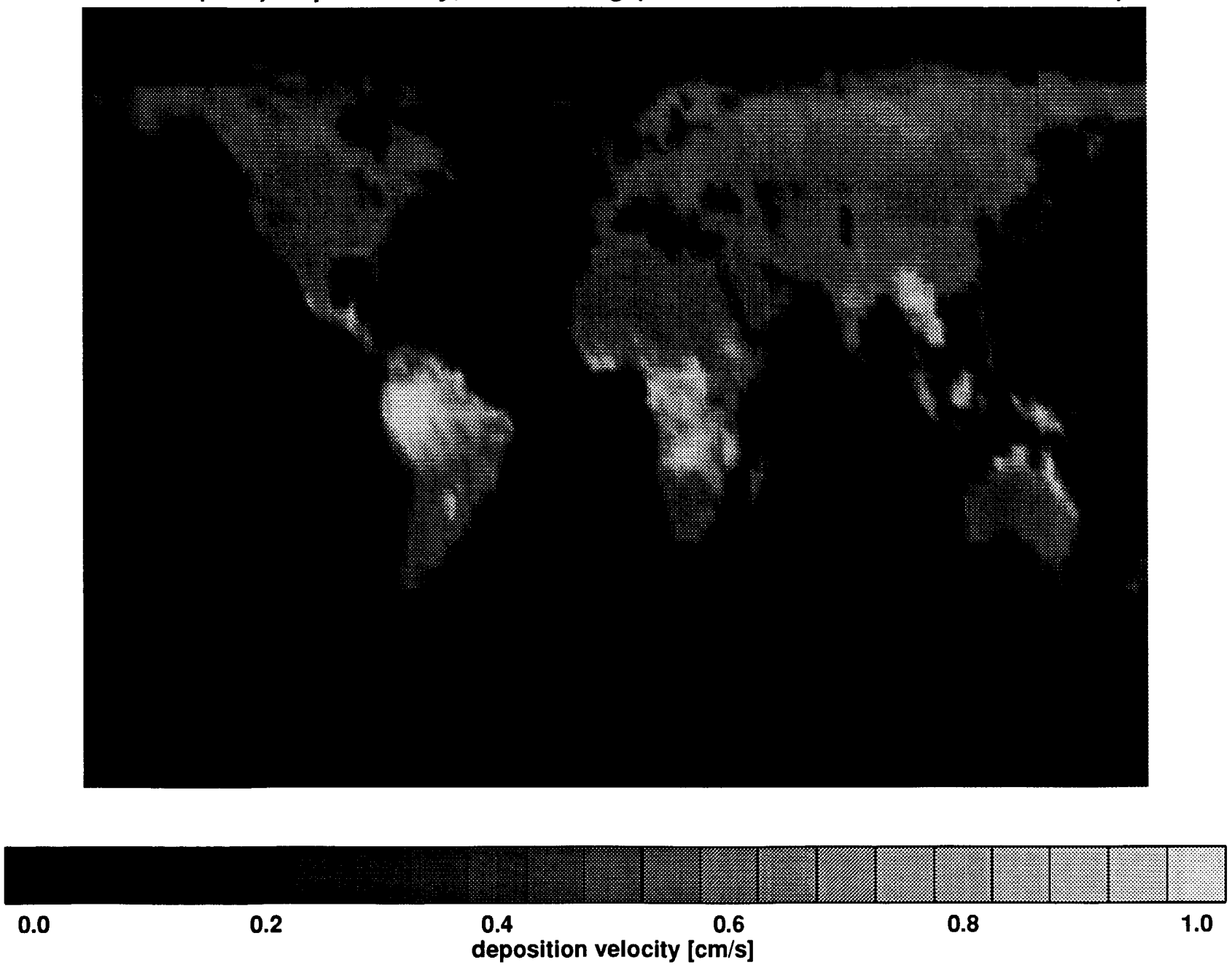
Ozone (JUL)-dep.-velocity, 2.8x2.8 deg (based on ds.769 & LARC snow/ice)
0.0
0.2
0.4
0.6
0.8
1.0
deposition velocity [cm/s]

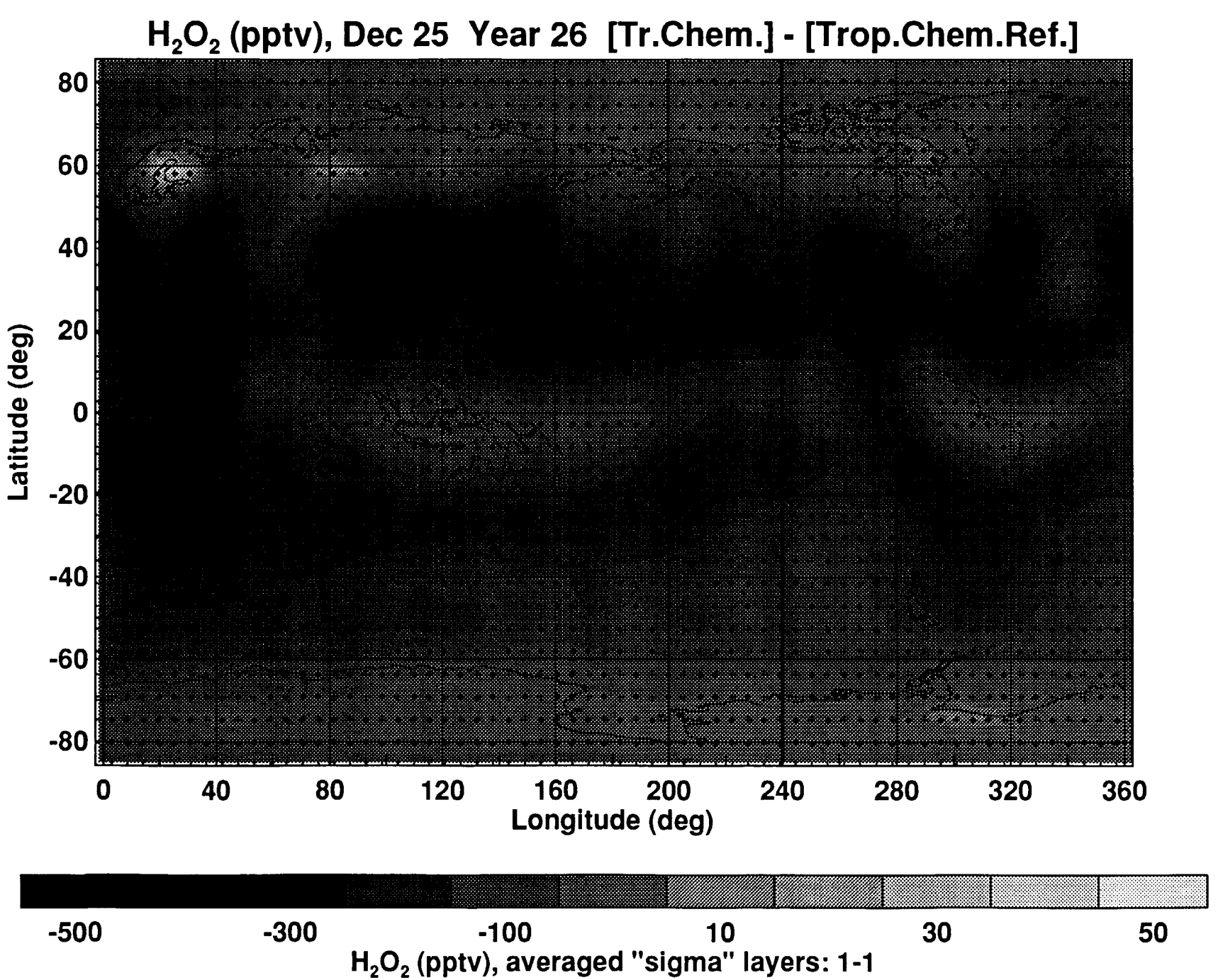
H2O2 (pptv), Dec 25 Year 26 [Tr.Chem.] - [Trop.Chem.Ref.]
Latitude (deg)
80
60
40
20
0
-20
-40
-60
-80
0
40
80
120
160
200
240
280
320
360
Longitude (deg)
-500
-300
-100
10
30
50
H2O2 (pptv), averaged "sigma" layers: 1-1

Fig 5a

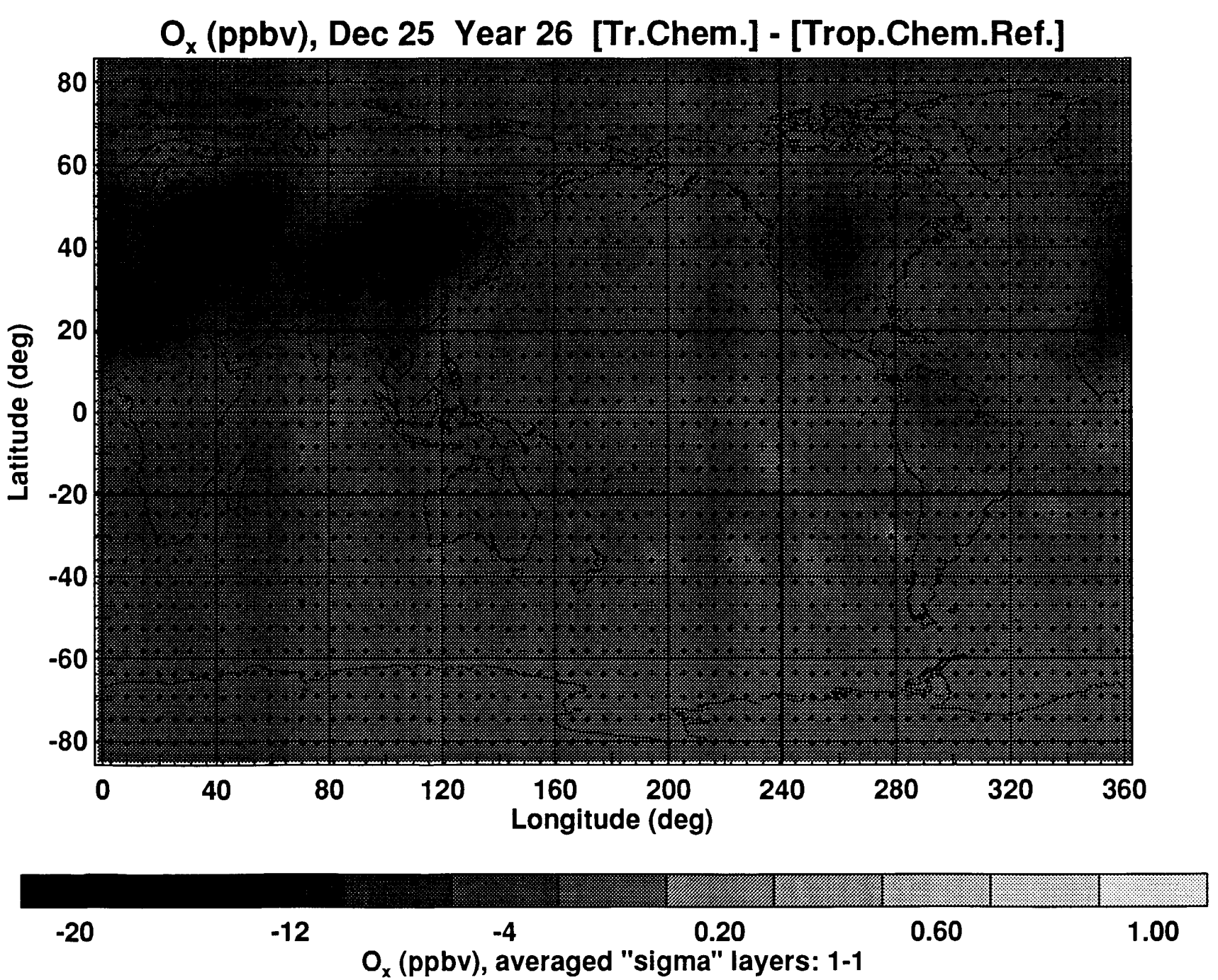
O_x (ppbv), Dec 25 Year 26 [Tr.Chem.] - [Trop.Chem.Ref.]
Latitude (deg)
80
60
40
20
0
-20
-40
-60
-80
0
40
80
120
160
200
240
280
320
360
Longitude (deg)
-20
-12
-4
0.20
0.60
1.00
O_x (ppbv), averaged "sigma" layers: 1-1

95 84

Ratio of O3 loss rates: NO vs NOx added = RLO_3

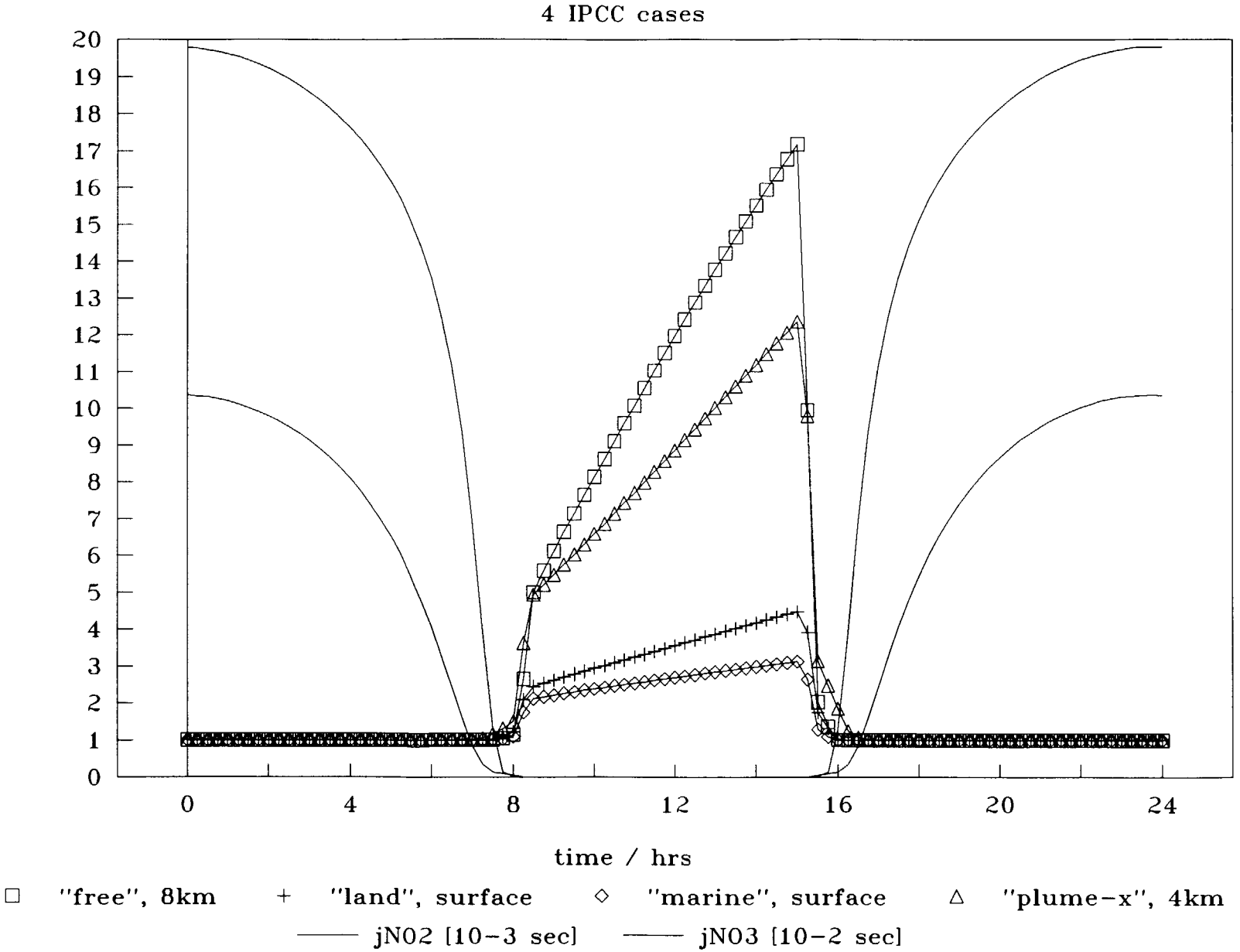

9 Pg

Comparison of Integration Steps

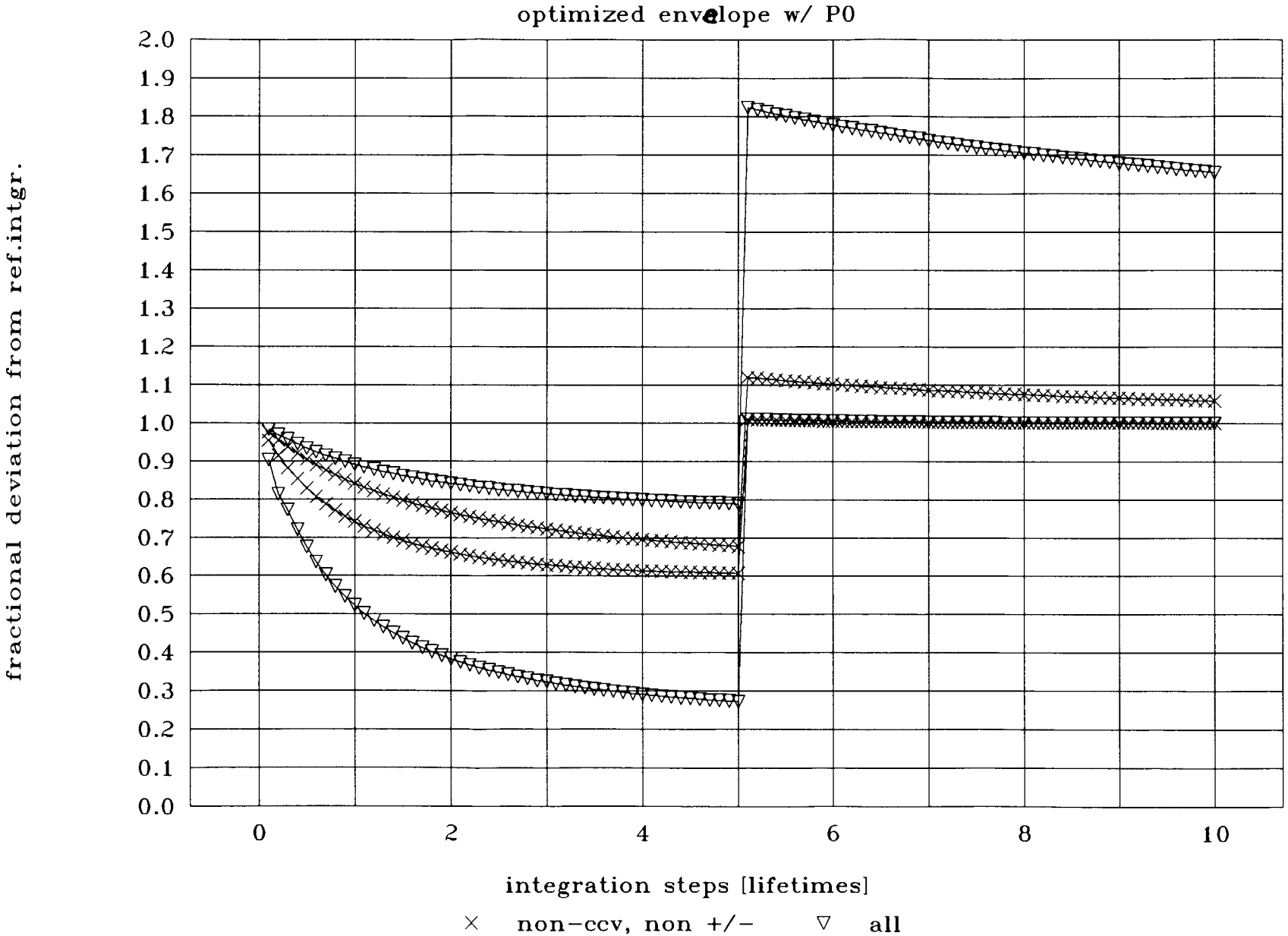

L 84

Comparison of Integration Steps

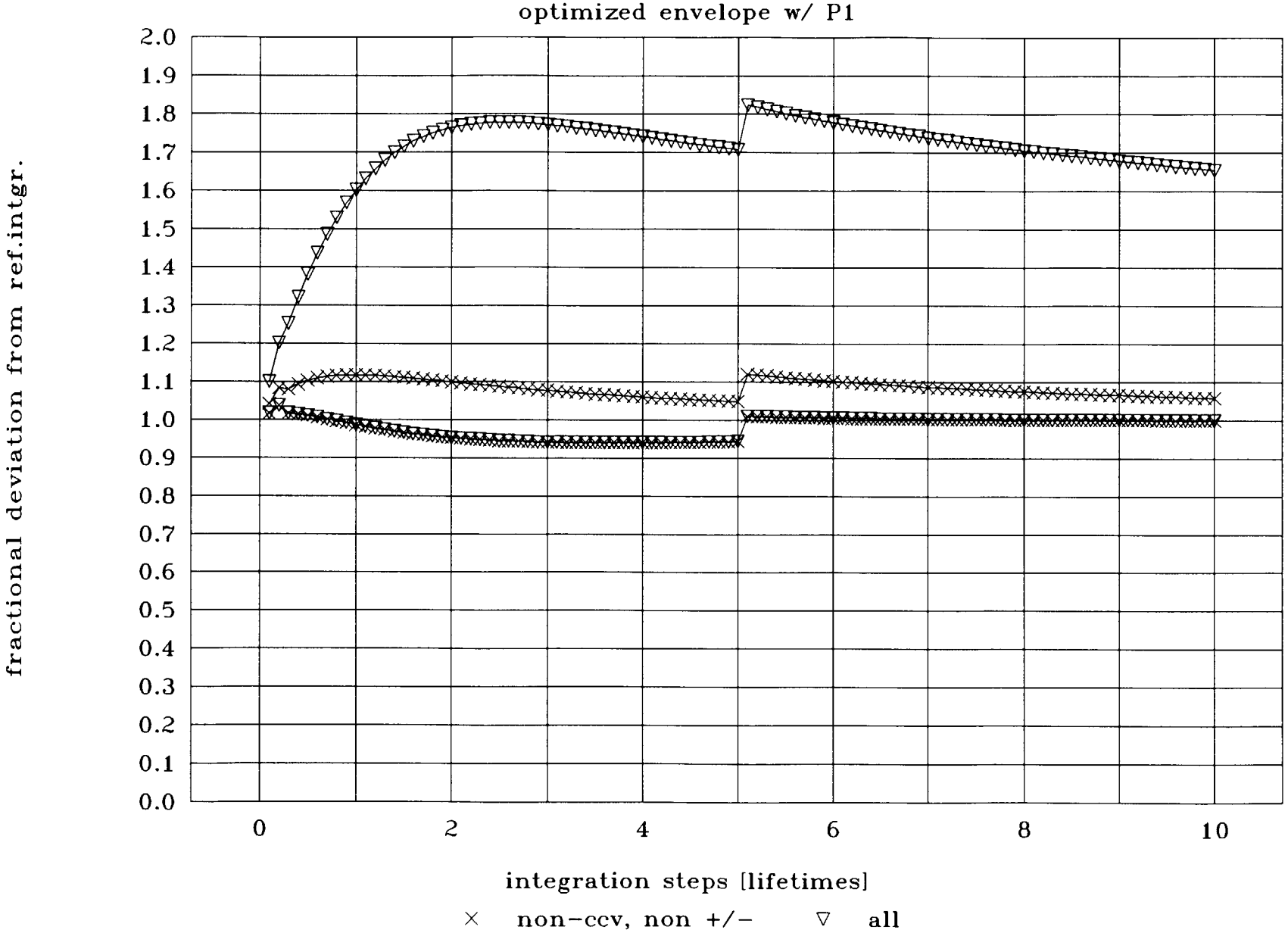

8 of 44

Comparison of Integration Steps

optimized envelope w/ P1 <-> (P0+P1)/2

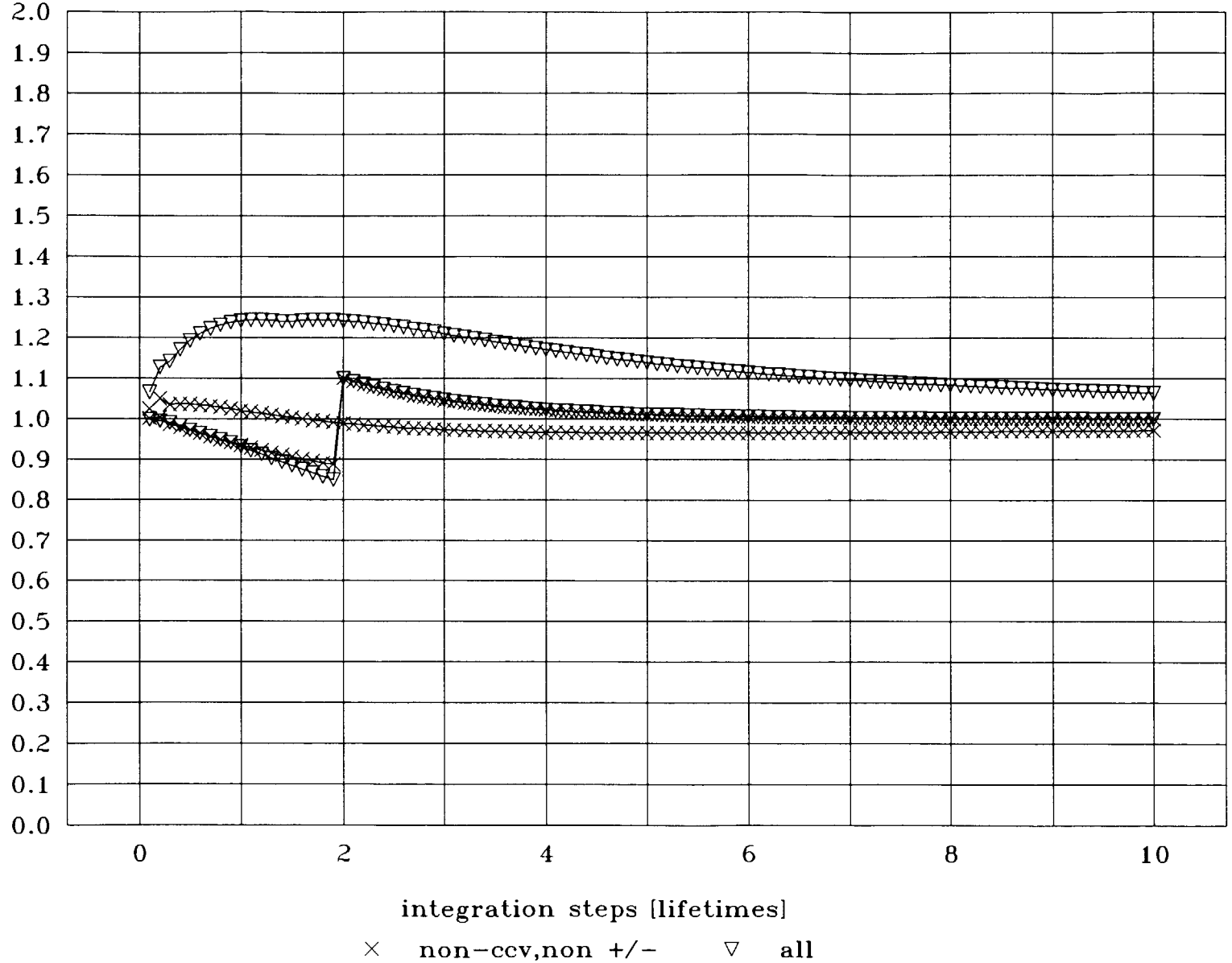

6 of 9